Anomalous features of particle production in high-multiplicity events of pp collisions at the LHC energies

Samrangy Sadhu and Premomoy Ghosh*

Variable Energy Cyclotron Centre, HBNI, 1/AF Bidhan Nagar, Kolkata 700 064, India

(Received 17 December 2018; published 22 February 2019)

Prevalent models of multiparticle production in relativistic pp collisions at pre-LHC energies fail to provide convincing explanations of certain significant features of the final-state charged particles in high-multiplicity pp events at the LHC. In this article we study these features—which are usually interpreted as the collective behavior of particle production in relativistic heavy-ion collisions—in the framework of the hydrodynamic EPOS3 model, emphasizing a quantitative comparison between the data and model-based simulations in the same kinematic ranges for better understanding of the data. The work reveals a quantitative mismatch between the data and the model.

DOI: 10.1103/PhysRevD.99.034020

I. INTRODUCTION

The experiments at the Relativistic Heavy Ion Collider (RHIC), through satisfactory descriptions of the flow-like behavior of particle production in relativistic heavy-ion collisions by relativistic hydrodynamics [1], established [2–5] the formation of a collective medium in such collisions. The suppression of high-p_T particles, revealed in terms of the relative yield of charged particles in heavy-ion collisions compared to pp collisions at the same center-of mass energy, identified the collective medium as a thermalized medium of quark-gluon plasma (QGP) [6,7]. Reconfirming the formation of the QGP with heavier ions at higher collisional energies, the experiments at the Large Hadron Collider (LHC) reported flow-like features of particle production in high-multiplicity events of pp collisions, in contrast to the present understanding of particle production in relativistic pp collisions based on the data from the pre-LHC energy range. It is the so-called "ridge" structure in the long-range near-side angular correlations in high-multiplicity events of proton-proton collisions at $\sqrt{s} = 7$ TeV that first distinguished [8] the anomaly in particle production in pp collisions at the LHC. Further experimental studies [9–11] at $\sqrt{s} = 7$ and 13 TeV confirmed the anomaly by extracting the elliptic flow coefficient v_2, the mass ordering of $v_2(p_T)$ for identified charged particles [11], and the p_T dependence of v_2 [9]. Similar unexpected features of particle production have also been observed in pPb collisions at $\sqrt{s_{NN}} = 5.02$ TeV [12–15] at the LHC. Subsequently, the RHIC data on dAu collisions uphold [16] the LHC observation of collective properties in particle production from small systems. The observation of elliptic and triangular flow patterns of charged particles produced in pAu, dAu, and ^{3}HeAu collisions at $\sqrt{s_{NN}} = 200$ GeV have been reported [17] to be best described by hydrodynamic models, which include the formation of a short-lived QGP droplet. Theoretically, the appearance of a "ridge" structure in high-multiplicity pp events at 7 TeV has been shown [18] to be expected in the hydrodynamic approach, based on flux tube initial conditions. The observation of the collective behavior of particle production in high-multiplicity pp events was further corroborated with the strong transverse radial flow extracted [19] from the satisfactory description of identified charged particle yields [20] from high-multiplicity pp events by the hydrodynamics-motivated Boltzmann-Gibbs blast-wave (BGBW) model [21]. Several other theoretical and phenomenological studies [22–26] indicated the possibility of a hydro-like collective medium in high-multiplicity pp events. Despite all of these studies that point towards the collective behavior of particle production in high-multiplicity events of small systems, the idea of connecting these anomalous features with the established hydro-like features of particle production from the QGP-like thermalized medium has not been unanimously accepted, due to the nonobservance of signal of suppression of high-p_T particles or any other compelling signal of the formation of the medium. Further, while several models in different approaches can qualitatively describe the data, it becomes difficult to make conclusions about the physical origin of particle production. Thus, the source of the "collective" or flow-like features in small systems remains ambiguous and invites thorough

*prem@vecc.gov.in

Published by the American Physical Society under the terms of the Creative Commons Attribution 4.0 International license. Further distribution of this work must maintain attribution to the author(s) and the published article's title, journal citation, and DOI. Funded by SCOAP³.

studies involving quantitative comparisons of the data in the light of several existing models of particle production in relativistic pp collisions.

This article presents a comprehensive study of high-multiplicity pp events at $\sqrt{s} = 7$ and 13 TeV, comparing the data with EPOS3 [27] generated simulated events, with the aim of understanding the anomalous features of particle production in pp collisions at the LHC. The EPOS3 simulation generates events with and without hydrodynamical evolution. The hydrodynamic EPOS3 event generator follows a similar particle production mechanism in pp, p-nucleus and nucleus-nucleus collisions, and thus has become a suitable testing ground for understanding the observed flow-like features in the high-multiplicity pp and pPb events at the LHC in comparison with the well-studied collective phenomena in relativistic nucleus-nucleus collisions. In the following section, we briefly describe the event generator. We analyze the EPOS3-generated events and present the results in Sec. III, in terms of the experimental observables which exhibit the flow-like effects in high-multiplicity pp events, namely, i) the two-particle azimuthal correlations among charged particles, ii) the blast-wave description of identified charged particles, iii) the mean transverse momentum ($\langle p_T \rangle$) as a function of the mean charged multiplicity ($\langle N_{\rm ch} \rangle$), and iv) the inverse slope parameter of the transverse mass (m_T) distribution. All of these observables are related to the transverse momentum of produced particles, collectively presented as the inclusive charged particle transverse momentum spectra. Before carrying out a differential analysis of the generated events in terms of these observables for a closer comparison with the data on an equal basis, the measured inclusive charged particle transverse momentum spectra for pp collisions at $\sqrt{s} = 7$ and 13 TeV are matched with those obtained from simulated events to ensure that the simulation code is, at least, minimally tuned. We summarize and conclude in Sec. IV.

II. EVENT GENERATOR

The details of the EPOS3 model parameters were discussed in the Ref. [27]. The model is known as parton-based Gribov-Regge theory. In the Gribov-Regge multiple scattering framework, an individual scattering—referred to as a Pomeron—gives rise to a parton ladder that consists of a hard perturbative QCD (pQCD) scattering along with initial-state and final-state parton emission. The parton ladder may be considered as a longitudinal color field or a flux tube, carrying the transverse momentum of the hard scattering. The flux tubes expand and are eventually fragmented into string segments of quark-antiquark pairs. In the case of many elementary parton-parton hard scatterings in a collision, a large number of flux tubes are formed leading to a high local string-segment density, and subsequently high multiplicity of the collisional event. In the hydrodynamic EPOS3 model, the high local string-segment density, above a critical value, constitutes the bulk matter or a medium. The string segments that do not have enough energy to escape from the bulk matter form the "core" which gets thermalized and undergoes $(3 + 1\text{D})$ viscus hydrodynamical evolution with a lattice-QCD-complied crossover equation of state, and the ratio of the shear viscosity and entropy density η/s is taken as 0.08. The hydrodynamical evolution is followed by particle production via the Cooper-Frye mechanism. After that, the hadronic evolution takes place and the "soft" (low-p_T) hadrons freeze out. The string segments from outside the bulk matter form the "corona." The string segments in the "corona" hadronize via the Schwinger mechanism and escape as "high"-p_T jet hadrons. The string segments carrying enough energy to escape the bulk matter constitute the "semihard" or intermediate-p_T particles. These segments, while escaping the bulk matter, pick up quarks or antiquarks from within the bulk matter, and the intermediate-p_T hadrons thus produced in this process inherit the properties of the bulk matter. After hadronization, the hadron-hadron rescattering is modeled via ultrarelativistic quantum molecular dynamics (UrQMD).

Using the EPOS 3.107 code, we have generated 40 million minimum-bias pp events for center-of-mass energies 7 and 13 TeV, for each of the options, with and without hydrodynamics. As presented in Fig. 1, our simulated event sample from the hydrodynamic EPOS3 model successfully describes the inclusive charged particle spectra from pp collisions at $\sqrt{s} = 7$ [28] and 13 TeV [29]. We analyze the same sample of events in terms of the discussed observables. Suitable subsamples of different multiplicity classes and different kinematic cuts are selected from the simulated minimum-bias event samples.

III. ANALYSIS AND RESULTS

A. Long-range ridge-like correlations

It will be pertinent to mention here, once again, that the "ridge-like" two-particle long-range angular correlations—a signal of the collective behavior of particle production in heavy-ion collisions as observed in pp collision data at $\sqrt{s} = 7$ TeV—could be qualitatively generated [17] in a "flux-tube + hydro" approach, similar to the approach adopted in the EPOS code. Despite the ability of the hydrodynamic approach to generate successful qualitative descriptions, a quantitative comparison with the data is essential, particularly to understand how the hydrodynamic description (implemented in EPOS) works better than the nonhydrodynamic models, including the reasonably well-understood particle production mechanism in the pQCD-inspired multiple parton interaction (MPI) model, like the one implemented in the PYTHIA Monte Carlo code.

The two-particle angular correlation function is defined by the per-trigger associated yields of charged particles obtained from the $\Delta\eta$, $\Delta\varphi$ distribution [where $\Delta\eta$ and $\Delta\varphi$

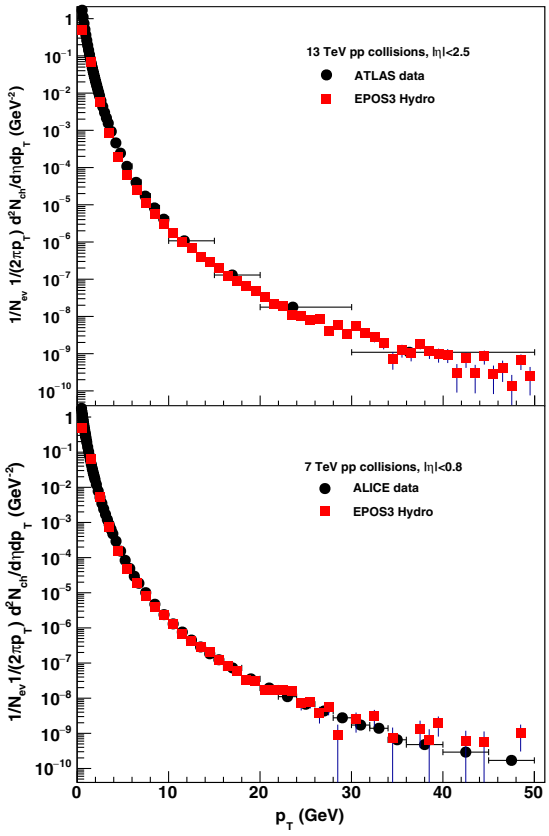

FIG. 1. Inclusive transverse momentum spectra of charged particles from generated minimum-bias events of pp collisions at $\sqrt{s} = 7$ and 13 TeV from the EPOS3 event generator, with hydrodynamic calculations, are compared with data, as measured by the ALICE [28] (lower panel) and ATLAS [29] (upper panel) experiments, respectively.

are the differences in the pseudorapidity (η) and azimuthal angle (φ) of the two particles] and is given by

$$\frac{1}{N_{\rm trig}}\frac{d^2N^{\rm assoc}}{d\Delta\eta d\Delta\varphi} = B(0,0) \times \frac{S(\Delta\eta,\Delta\varphi)}{B(\Delta\eta,\Delta\varphi)}, \tag{1}$$

where $N_{\rm trig}$ is the number of trigger particles in the specified $p_T^{\rm trigger}$ range.

The function $S(\Delta\eta,\Delta\varphi)$ is the differential measure of the per-trigger distribution of associated hadrons in the same event, i.e.

$$S(\Delta\eta,\Delta\varphi) = \frac{1}{N_{\rm trig}}\frac{d^2N^{\rm assoc}_{\rm same}}{d\Delta\eta d\Delta\varphi}. \tag{2}$$

The background distribution function $B(\Delta\eta,\Delta\varphi)$ is defined as

$$B(\Delta\eta,\Delta\varphi) = \frac{d^2N^{\rm mixed}}{d\Delta\eta d\Delta\varphi}, \tag{3}$$

where $N^{\rm mixed}$ is the number of mixed event pairs.

The factor $B(0,0)$ in Eq. (1) is used to normalize the mixed-event correlation function such that it is unity at $(\Delta\eta,\Delta\varphi) = (0,0)$.

The study of the two-particle azimuthal correlations allows to extract several sources of correlations in multiparticle production, depending on the studied ranges of $|\Delta\eta|$ and also the p_T for the trigger and the associated particles. In the context of the present study, the correlated emission of particles from the collective medium can be extracted by studying the long-range ($|\Delta\eta| \gg 0$) two-particle azimuthal angle correlations. In relativistic heavy-ion collisions, the long-range two-particle azimuthal angle correlations are attributed to the formation of the collective medium. The correlated pair yields per trigger with small $|\Delta\varphi|$ over a wide range of $|\Delta\eta|$ (long range) result in a "ridge" structure in the constructed correlation functions. The analysis [10] of LHC pp data in terms of correlated yields as a function of $|\Delta\varphi|$ revealed that the "ridge"-structure becomes prominent in pp collisions with increasing event multiplicity. It is the near-side ($|\Delta\varphi| \sim 0$) long-range correlations that are of particular interest for the present study on a quantitative comparison between the data and the hydrodynamic simulation of multiparticle production in high-multiplicity pp events.

We construct the long-range two-particle angular correlations of the charged particles in simulated events, matching the kinematic cuts and multiplicity classes as chosen for the analysis of the data in Ref. [10] for $\sqrt{s} = 7$ and 13 TeV. As expected from a hydrodynamic code of particle production like the EPOS3-hydro, the long-range two-particle azimuthal correlations of charged particles reveal a prominent ridge-like structure for high-multiplicity events, while such a structure is absent for low-multiplicity events. Figure 2 contains representative plots of the two-particle correlation function for $1 < p_T^{\rm trigger}$, $p_T^{\rm associated} < 2$ GeV/c with an unidentified charged particle as the trigger, for the hydrodynamic-EPOS3-generated pp collisions at $\sqrt{s} = 7$ TeV for events of multiplicity classes $N_{\rm ch} > 110$ and $N_{\rm ch} < 35$, after removing the short-range jet-like correlations. The per-trigger correlated yield for representative high-multiplicity event classes in different p_T intervals, for both the nonhydrodynamic- and hydrodynamic- EPOS3-generated pp collisions at $\sqrt{s} = 7$ and 13 TeV, are projected onto $\Delta\varphi$ after subtracting the "zero yield at minimum" $Yield_{|\rm ZYAM|}$ [10], and are shown in Figs. 3 and 4, respectively, to compare the data in the same kinematic ranges.

The appearance of the ridge-like structure in the long-range two-particle angular correlations of the charged particles in the high-multiplicity EPOS3-hydro generated pp events at $\sqrt{s} = 7$ and 13 TeV reflects the collective

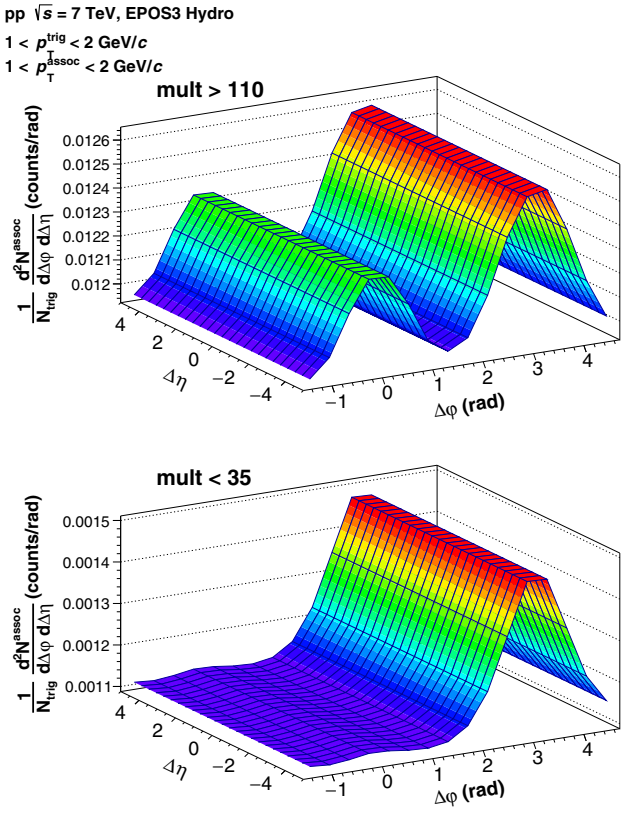

FIG. 2. Two-particle $\Delta\eta - \Delta\varphi$ charged particle correlation function for $1 < p_T^{\text{trigger}}$, $p_T^{\text{associated}} < 2$ GeV/c with an unidentified charged particle as the trigger, for the hydrodynamic- EPOS3-generated pp collisions at $\sqrt{s} = 7$ TeV for events of multiplicity class $N_{\text{ch}} > 110$ (upper panel) and $N_{\text{ch}} < 35$ (lower panel). The short-range correlations have been suppressed in order to clearly present the long-range correlations.

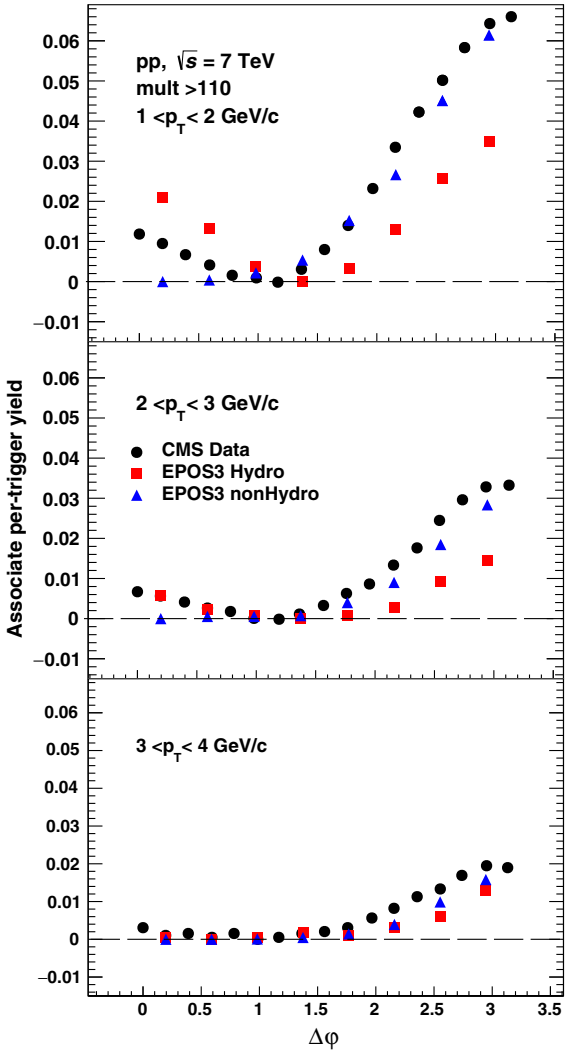

FIG. 3. One-dimensional $\Delta\varphi$ projection of high-multiplicity events for the region of ridge-like correlations obtained from the long-range two-particle azimuthal correlations of charged particles, averaged over $2 < |\Delta\eta| < 4$, for $1 < p_T^{\text{trigger}}$, $p_T^{\text{associated}} < 2$ GeV/c, $2 < p_T^{\text{trigger}}$, $p_T^{\text{associated}} < 3$ GeV/c, and $3 < p_T^{\text{trigger}}$, $p_T^{\text{associated}} < 4$ GeV/c from data [10] and the hydrodynamic EPOS3-generated events of pp collisions at $\sqrt{s} = 7$ TeV.

property, which is expected in a hydrodynamic model of particle production. The correlated yields of high-multiplicity event classes as a function of $\Delta\varphi$ for different p_T intervals in the simulated events reveal a similar feature as that observed in the two-particle azimuthal correlations of the charged particles in the data: the ridge-like structure is most prominent in the 1–2 GeV/c p_T range and in the highest-multiplicity events, while it gradually decreases with increasing p_T. Nevertheless, as is clear in Figs. 3 and 4, for the most prominent p_T range of 1–2 GeV/c, the EPOS3 events overestimate the correlated yields as compared to the data.

B. Blast-wave parametrization

In a hydrodynamic picture of relativistic collisions of heavy nuclei, the collective radial flow, generated due to the pressure gradient in the system, is reflected in the spectra of identified final-state charged particles produced in relativistic collisions. The BGBW model [21], a hydrodynamics-motivated empirical formalism, estimates the radial flow by analyzing the identified particle spectra. The blast-wave model considers that the particles produced in the collision are locally thermalized and the system expands collectively with a common velocity field. Though the model does not include hydrodynamic evolution, it considers that the system undergoes an instantaneous common freeze-out at a kinetic freeze-out temperature (T_{kin}) and a transverse radial flow velocity (β) at the freeze-out surface. The BGBW model, which has been thoroughly used in analyzing relativistic nucleus-nucleus collision data, has revealed [19] a transverse radial flow for high-multiplicity pp collision data as well [20].

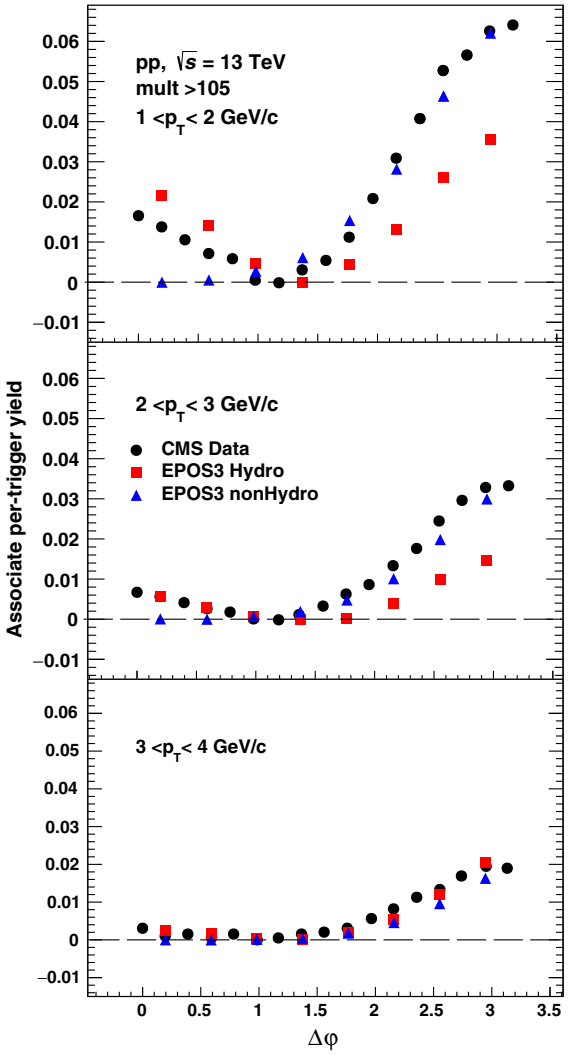

FIG. 4. Same as Fig. 3 for pp events at $\sqrt{s} = 13$ TeV.

Assuming a hard-sphere particle source of uniform density, the transverse momentum spectra in the BGBW model is given by

$$\frac{dN}{p_T dp_T} \propto \int_0^R r dr m_T \mathbf{I}_o\left(\frac{p_T \sinh\rho}{T_{\rm kin}}\right)\mathbf{K}_1\left(\frac{m_T \cosh\rho}{T_{\rm kin}}\right), \quad (4)$$

where $\rho = \tanh^{-1}\beta$, and $\mathbf{I}_0$ and $\mathbf{K}_1$ are modified Bessel functions.

The flow velocity profile is given by

$$\beta = \beta_s\left(\frac{r}{R}\right)^n, \quad (5)$$

where β_s is the surface velocity and r/R is the relative radial position in the thermal source. The average transverse flow velocity $\langle\beta\rangle$ is given by $\langle\beta\rangle = \frac{2}{(2+n)}\beta_s$.

The hydrodynamic- EPOS3-generated pp events are expected to exhibit a radial flow. Using the BGBW formalism, we intend to quantitatively compare the radial flow parameters for the EPOS3-generated events and the data. We use the chi-squared (χ^2) test to ensure the goodness of fit while obtaining the fit parameters, the kinetic freeze-out temperature, and the radial flow velocity from the spectra data as well as from the generated spectra. For our analysis, we put the lower p_T cut for the spectra of all species at 0.475 GeV/c. On the higher side, the p_T range is limited to $p_T < 2$ GeV/c or less, depending on the availability of the data.

We calculate R for different event classes with different $\langle N_{\rm ch}\rangle$ with $|\eta| < 2.4$ in this study, from the relation $R(\langle N_{\rm ch}\rangle) = a.\langle N_{\rm ch}\rangle^{1/3}$ where $a = 0.597 \pm 0.009(\text{stat}) \pm 0.057(\text{syst})$ fm at 0.9 TeV and $a = 0.612 \pm 0.007(\text{stat}) \pm 0.068(\text{syst})$ fm, as parametrized by the CMS experiment [20] from the measurement of the radius of the source of emission as a function of the average charged particle multiplicity for pp collisions at $\sqrt{s} = 7$ TeV. The BGBW fit parameters are available [19] for different multiplicity classes of pp collisions at $\sqrt{s} = 7$ TeV [20]. We fit the blast-wave function to the p_T spectra for different sets of data for $\sqrt{s} = 13$ TeV [30], keeping the kinetic freeze-out temperature ($T_{\rm kin}$), the radial flow velocity (β_s), and the exponent (n) of the flow velocity profile free to produce the best possible simultaneous or combined fits to the data, in terms of χ^2/d.o.f.

Figures 5 and 6 show the BGBW fits to the spectra data of identified particles from pp collisions at 7 TeV for the event classes with average multiplicities of 98 and 131,

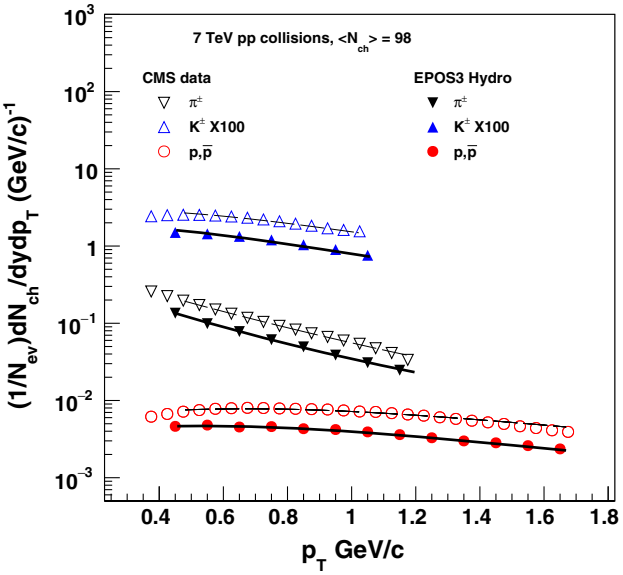

FIG. 5. The transverse momentum spectra for $\pi^{\pm}$, $K^{\pm}$, and $p(\bar{p})$ as measured by the CMS experiment [20] at the LHC for the event class with an average multiplicity of 98 in pp collisions at $\sqrt{s} = 7$ TeV, along with the BG-blast-wave fits (solid lines). The uncorrelated statistical and systematic uncertainties have been added in quadrature.

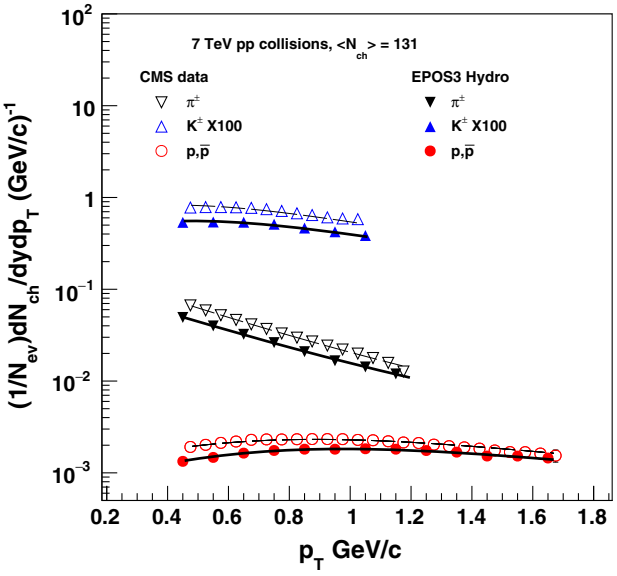

FIG. 6. The transverse momentum spectra for $\pi^{\pm}$, $K^{\pm}$, and $p(\bar{p})$ as measured by the CMS experiment [20] at the LHC for the event class with an average multiplicity of 131 in pp collisions at $\sqrt{s} = 7$ TeV, along with BG-blast-wave fits (solid lines). The uncorrelated statistical and systematic uncertainties have been added in quadrature.

respectively, along with the fits to the simulated spectra obtained from the respective classes of simulated events.

In Table I we list the fit parameters, the kinetic freeze-out temperature ($T_{\rm kin}$), the average radial flow velocity ($\langle\beta\rangle$) at the freeze-out surface, and the exponent (n) as obtained by a simultaneous fit of identified particle spectra using the BGBW model for different classes of high-multiplicity pp events and for $\sqrt{s} = 7$ and 13 TeV, along with their respective χ^2/d.o.f. The table includes parameters for those event classes that are fit reasonably well by the BW function. Table II presents similar results for the hydrodynamic- EPOS-generated events.

Figures 5 and 6 along with Tables I and II show that the data and the EPOS3-hydro generated events do not quantitatively agree in terms of the BW parameters, except for very-high multiplicity classes with average multiplicities of 151 and 162 in pp collisions at $\sqrt{s} = 13$ TeV.

C. $\langle p_T \rangle$ as a function of $\langle N_{\rm ch} \rangle$

The ALICE experiment at the LHC measured the $\langle p_T \rangle$ of charged particles as a function of $\langle N_{\rm ch} \rangle$ [31], in the pseudorapidity range $|\eta| < 1.0$ and with transverse momentum p_T up to 10 GeV/c, and showed that the data for pp collisions at $\sqrt{s} = 7$ TeV could be well described by the pQCD-inspired MPI model with color reconnection, as implemented in PYTHIA monte carlo code. We calculate the observables in the same kinematic ranges used by ALICE for the events generated with both the hydrodynamic and nonhydrodynamic EPOS3 simulations. The results along with the data are depicted in Fig. 7.

As is clear from Fig. 7, the EPOS3 code, with or without hydrodynamics, cannot describe the ALICE measurement of $\langle p_T \rangle$ as a function of $\langle N_{\rm ch} \rangle$. The ATLAS experiment [28] has studied the same for pp collisions at $\sqrt{s} = 13$ TeV, though in different kinematic ranges, $|\eta| < 2.4$ and $p_T > 0.5$ GeV/c. We repeat the analysis of $\langle p_T \rangle$ as a function of $\langle N_{\rm ch} \rangle$ in accordance with the kinematic cuts used for the ATLAS data. A comparison of the simulation and the data is presented in Fig. 8. The data and the simulated events do not match exactly in this case as well. It may be noted that both the ALICE and ATLAS data include particles with p_T much higher than the p_T range of the "soft" particles likely to be produced from the "core" or the bulk collective medium that is considered in the EPOS hydrodynamic code. In view of this, to compare the data of only the "soft" particles we choose the CMS data for identified p_T spectra from events in different multiplicity classes.

The CMS experiment has measured the p_T spectra of $\pi^{\pm}$, $K^{\pm}$, and $p(\bar{p})$ over the rapidity range $|y| < 1$ [$y = (1/2)\ln\frac{E+p_L}{E-p_L}$] for pp collisions at $\sqrt{s} = 7$ and

TABLE I. $T_{\rm kin}$, $\langle\beta\rangle$, and n—the parameters of the BGBW model—obtained from the simultaneous fit to the published [20,29] spectra of $\pi^{\pm}$, $K^{\pm}$, and $p(\bar{p})$ and their respective χ^2/d.o.f. for pp collisions at $\sqrt{s} = 7$ and 13 TeV for different event classes depending on average multiplicity $\langle N_{\rm ch} \rangle$ in the range $|\eta| < 2.4$.

$\sqrt{s}$ (TeV)	$\langle N_{\rm ch} \rangle$	$T_{\rm kin}$ (MeV)	$\langle\beta\rangle$	n	χ^2/d.o.f.
7	98	115.57 ± 0.11	0.766 ± 0.004	0.540 ± 0.006	1.02
7	109	113.09 ± 0.12	0.779 ± 0.004	0.503 ± 0.006	0.61
7	120	110.84 ± 0.15	0.790 ± 0.004	0.480 ± 0.006	0.34
7	131	104.29 ± 0.15	0.809 ± 0.005	0.436 ± 0.005	0.44
13	108	140.80 ± 0.022	0.723 ± 0.005	0.58 ± 0.01	1.65
13	119	129.31 ± 0.019	0.778 ± 0.002	0.56 ± 0.011	0.86
13	130	128.29 ± 0.019	0.763 ± 0.004	0.50 ± 0.009	1.18
13	141	119.77 ± 0.016	0.764 ± 0.004	0.48 ± 0.01	1.40
13	151	112.84 ± 0.016	0.783 ± 0.004	0.44 ± 0.011	1.44
13	162	102.67 ± 0.017	0.826 ± 0.003	0.36 ± 0.007	0.93

TABLE II. $T_{\rm kin}$, $\langle\beta\rangle$, and n—the parameters of the BGBW model—obtained from the simultaneous fit to the spectra obtained from simulated EPOS events for $\pi^{\pm}$, $K^{\pm}$, and $p(\bar{p})$ and their respective χ^2/d.o.f. for pp collisions at $\sqrt{s} = 7$ and 13 TeV for different event classes depending on average multiplicity $\langle N_{\rm ch}\rangle$ in the range $|\eta| < 2.4$.

$\sqrt{s}$ (TeV)	$\langle N_{\rm ch}\rangle$	$T_{\rm kin}$ (MeV)	$\langle\beta\rangle$	n	χ^2/d.o.f.
7	98	106.10 ± 0.015	0.768 ± 0.0003	0.59 ± 0.001	30.83
7	109	105.91 ± 0.008	0.808 ± 0.001	0.46 ± 0.005	1.51
7	120	103.30 ± 0.01	0.813 ± 0.002	0.45 ± 0.003	1.59
7	131	103.02 ± 0.02	0.829 ± 0.002	0.39 ± 0.004	0.52
13	108	142.00 ± 0.002	0.749 ± 0.001	0.63 ± 0.01	7.54
13	119	142.00 ± 0.0019	0.774 ± 0.005	0.50 ± 0.002	0.86
13	130	141.96 ± 0.006	0.774 ± 0.008	0.45 ± 0.009	1.16
13	141	127.98 ± 0.016	0.797 ± 0.001	0.44 ± 0.004	1.31
13	151	112.90 ± 0.01	0.814 ± 0.006	0.43 ± 0.004	0.96
13	162	100.52 ± 0.015	0.815 ± 0.007	0.42 ± 0.007	1.43

13 TeV $|\eta| < 2.4$. The measured p_T ranges for the measured identified particles in pp collisions at both 7 [20] and 13 TeV [30] are 0.1–1.2 GeV/c for $\pi^{\pm}$, 0.2–1.05 GeV/c for $K^{\pm}$, and 0.35–1.7 GeV/c for p and $\bar{p}$. The measured p_T ranges fall within the p_T range of EPOS3 for particles originating from the hydrodynamic bulk medium.

We compute $\langle p_T\rangle$ from the CMS data for identified charged particle spectra for different event classes from pp collisions at $\sqrt{s} = 7$ [20] and 13 TeV [30]. It is clear from Fig. 9 that for pp collision data at 7 TeV the $\langle p_T\rangle$ values of the majority of produced "soft" particles (the pions) in the simulated events do not match the measured ones in the given kinematic range. For pp collisions at 13 TeV, the mismatch between the data and the simulated events, as shown in Fig. 10, is rather wide for all of the identified particles.

D. Multiplicity-dependent inverse slope parameter of m_T distributions

The slope of the transverse mass m_T spectra of identified particles contains information about the temperature of the medium (if present) that produces the particles, and the effect of the transverse expansion of the medium. We obtain the m_T spectra of identified charged particles of mass m for different high-multiplicity classes of pp events at $\sqrt{s} = 7$ and 13 TeV from the p_T spectra measured [20,30] by the CMS experiments from the relation $m_T = (m^2 + p_T^2)^{1/2}$.

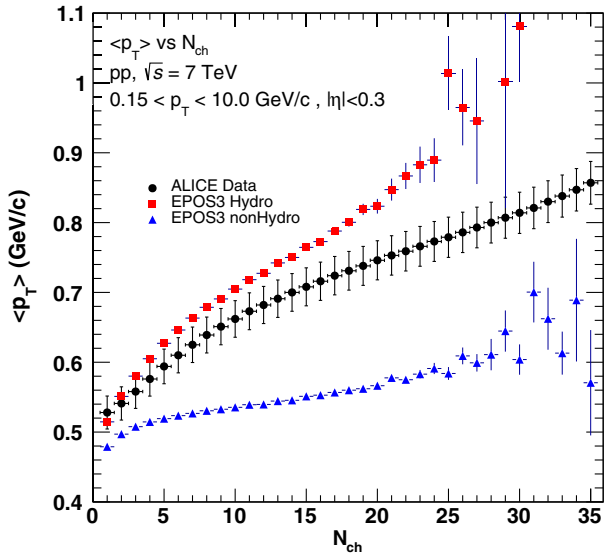

FIG. 7. The average transverse momentum $\langle p_T\rangle$ as a function of charged particle multiplicity $N_{\rm ch}$ as measured by ALICE [31] is compared with the simulated events from the EPOS3 event generator, with and without hydrodynamic calculations.

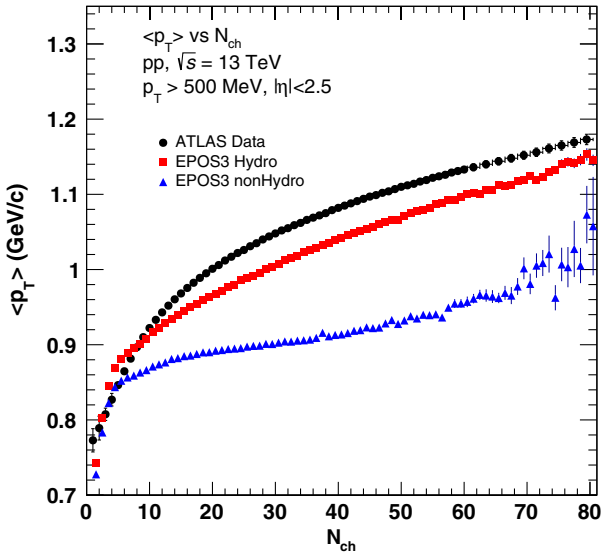

FIG. 8. The average transverse momentum $\langle p_T\rangle$ as a function of charged particle multiplicity $N_{\rm ch}$ as measured by ATLAS [28] is compared with the simulated events from the EPOS3 event generator, with and without hydrodynamic calculations.

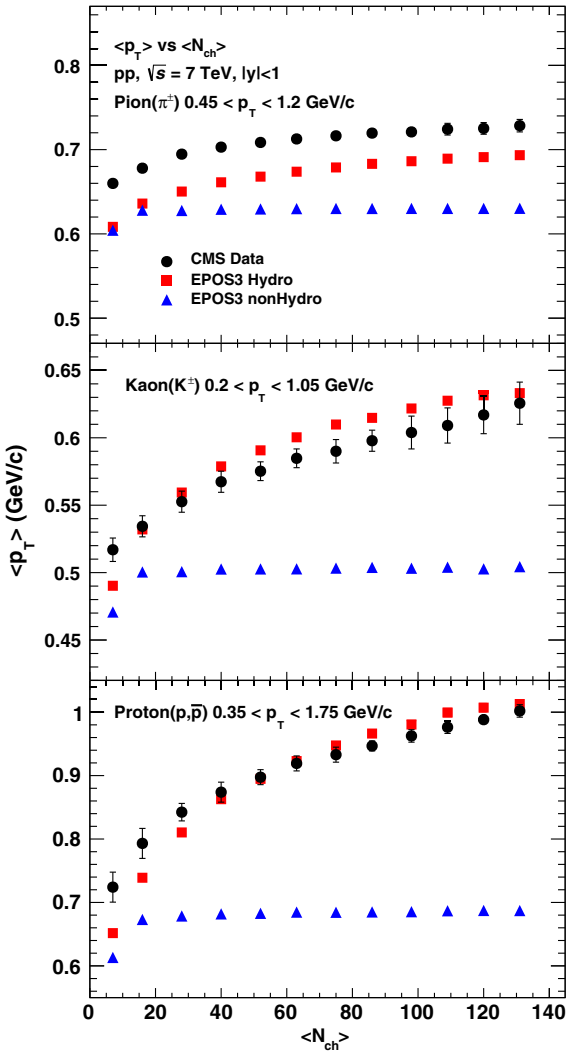

FIG. 9. Average transverse momentum $\langle p_T \rangle$ as a function of mean charged particle multiplicity $\langle N_{\rm ch} \rangle$ for the identified charged particles in pp collisions at $\sqrt{s} = 7$ TeV. The CMS data [20] are compared with simulated events using the EPOS3 event generator, with and without hydrodynamics.

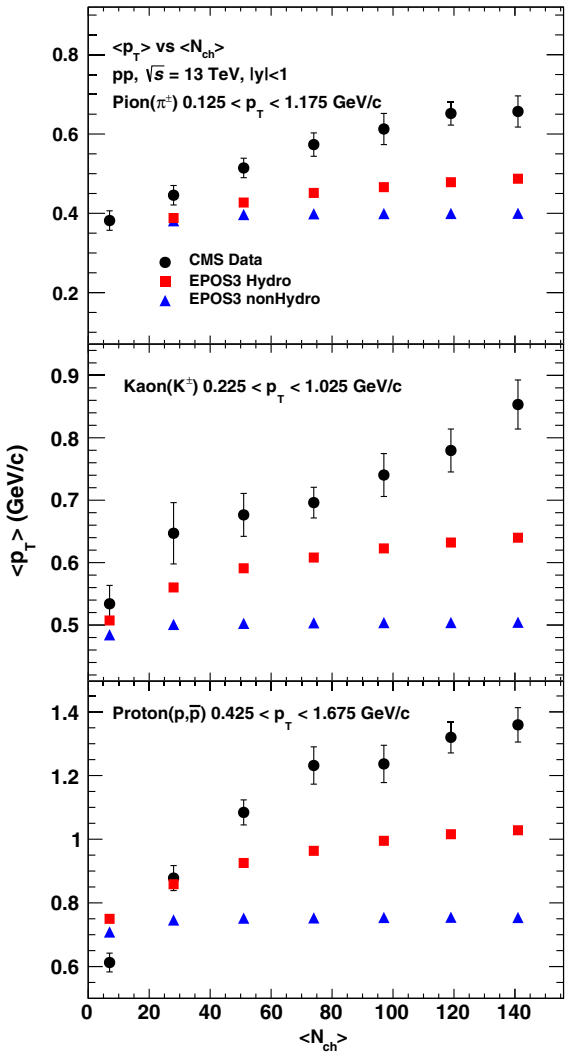

FIG. 10. Average transverse momentum $\langle p_T \rangle$ as a function of mean charged particle multiplicity $\langle N_{\rm ch} \rangle$ for the identified charged particles in pp collisions at $\sqrt{s} = 13$ TeV. The CMS data [30] are compared with simulated events using the EPOS3 event generator with and without hydrodynamics.

The m_T spectra are fitted in the range corresponding to low p_T with the exponential function

$$\frac{dN}{m_T dm_T} = C.\exp\left(-\frac{m_T}{T_{\rm effective}}\right), \tag{6}$$

where $T_{\rm effective}$, the inverse slope parameter, contains the effect due to the transverse expansion of the system. The increase in the inverse slope parameter $T_{\rm effective}$ for the most commonly measured identified particles ($\pi^{\pm}$, $K^{\pm}$, p, and $\bar{p}$), as has been observed in heavy-ion collisions [32,33] is attributed to the collective transverse flow of the medium formed in the collision. An increase in the inverse slope parameters has also been observed in high-multiplicity event classes of pPb collisions at $\sqrt{s_{NN}} = 5.02$ TeV [34] and pp collisions at $\sqrt{s} = 7$ [35].

We fit the m_T spectra of identified particles in the overlap range ($0.475 < p_T < 1.025$) of p_T spectra at $\sqrt{s} = 7$ and 13 TeV obtained from the data [20,30] as well as from the EPOS3-hydro simulation for the high-multiplicity event classes. The inverse slope parameters obtained from the best fit of the spectra (in terms of χ^2/d.o.f.) using the MINUTE program in the ROOT analysis framework [29] are presented in Figs. 11 and 12 for some representative high-multiplicity event classes.

From Figs. 11 and 12 it is clear that while the EPOS3-hydro high-multiplicity pp events exhibit mass ordering of inverse slope parameter of the m_T distributions, they largely deviate from those obtained from the measured spectra.

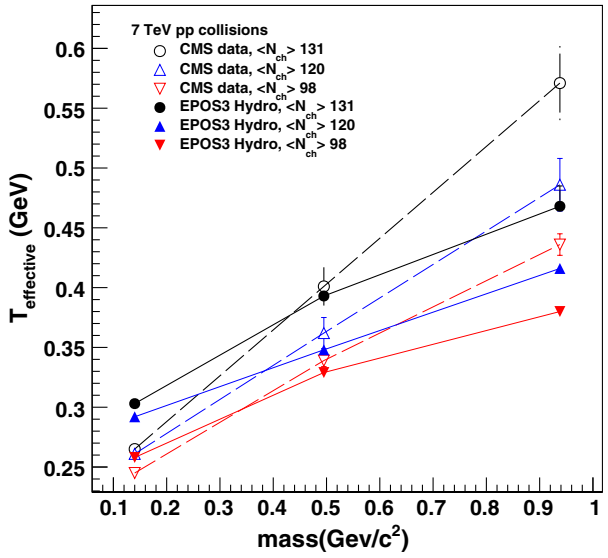

FIG. 11. The mass ordering of the inverse slope parameter $T_{\text{effective}}$ of identified particles ($m_{\pi^{\pm}} = 0.14$, $m_{K^{\pm}} = 0.495$, $m_{p(\bar{p})} = 0.938$ GeV/c^2) as measured by the CMS experiment [20] at $\sqrt{s} = 7$ TeV for a few high-multiplicity event classes is compared with those obtained from EPOS3-hydro simulated events. $\langle N_{\text{ch}} \rangle$ is the mean multiplicity of the charged particles of each respective event class.

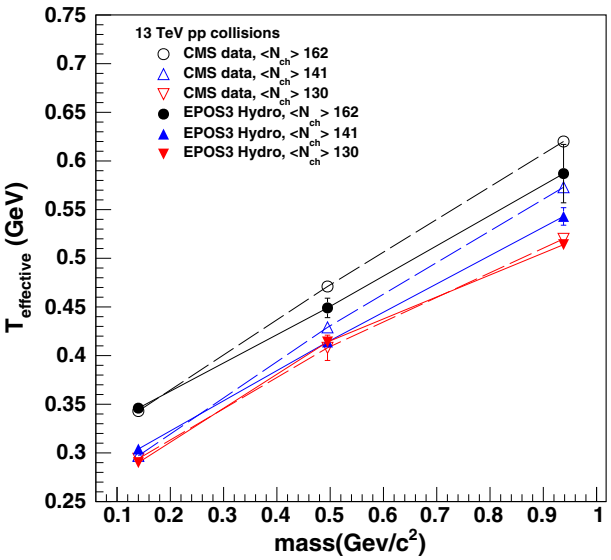

FIG. 12. Same as Fig. 11 for CMS data [30] and EPOS3-simulated events of pp collisions at $\sqrt{s} = 13$ TeV.

IV. SUMMARY AND CONCLUSION

In the context of several experimental signatures of the collective nature of particle production in relativistic collisions of small systems at the RHIC and LHC, we analyzed simulated pp events at $\sqrt{s} = 7$ and 13 TeV using the EPOS3-hydro code—a hydrodynamic model of particle production—for different systems of relativistic collisions in order to quantitatively compare them with the particle production data in high-multiplicity pp events, so as to better understand the experimental signals.

We studied the multiplicity dependence of the long-range two-particle angular correlations of charged particles produced in EPOS3-generated pp events. The EPOS3-hydro-generated high-multiplicity events reveal a"ridge-like" structure, which is most prominent in the 1–2 GeV/c p_T range and gradually decreases with increasing p_T. The diminishing trend of the correlated yield with increasing p_T is similar to what is observed in the data. However, the EPOS3 events overestimate the correlated yields. The kinetic freeze-out temperature (T_{kin}) and the transverse radial flow velocity (β) at the freeze-out surface as obtained from the blast-wave fits to the identified particle spectra for high-multiplicity event classes of EPOS3-simulated events do not match the parameters for the data. The mean transverse momentum as a function of multiplicity for all charged particles and as a function of the mean multiplicity for identified charged particles from EPOS3-generated events, in different kinematic ranges, vary widely from those measured for 13 TeV pp data at the LHC. Although the inverse slope parameters obtained from exponential fits to the transverse mass spectra of EPOS3-generated events exhibit the expected mass ordering from the hydrodynamic model of particle production, the values of the parameters do not agree with those obtained from the data.

This data-driven study has revealed that, although the EPOS3 hydrodynamic model may reasonably describe the nature of some of the average bulk features that reflect the collective properties of particle production in the high-multiplicity pp events at the LHC, it cannot match the data quantitatively. Given the quantitative mismatch in terms of the studied observables related to the transverse momentum of the particles, one would also expect a quantitative mismatch in terms of the fundamental observable: the inclusive spectra of the invariant yields of produced particles. In this respect, the EPOS3 code appears to be inconsistent. The quantitative mismatch, however, cannot undermine the qualitative agreement of the EPOS3 simulation with the data. As has already been shown [35] in a study on identified particle spectra data [20] of pp collisions at 7 TeV, both EPOS versions (EPOS3 and EPOS-LHC) match the trend of the data better than the conventional nonhydrodynamic event generators, including PYTHIA [36]. In contrast to PYTHIA, the EPOS simulations include the flow of produced particles. The EPOS-LHC contains a parametrized collective flow at the freeze-out, and the advanced version of EPOS3 contains a full (3D + 1) viscous hydrodynamic simulation. The better matching of the particle spectra data by EPOS simulations as compared to the conventional pp simulation codes establishes the collective behavior of pp data at the LHC. Nevertheless, in the scenario where several other hydrodynamic as well as nonhydrodynamic models qualitatively reproduce the

so-called collective features of particle production in high-multiplicity events of small collision systems, quantitative descriptions of as many observables as possible in a consistent framework/model is desirable in order to identify the origin of these features. This study may be useful for further tuning of the EPOS3 input parameters, in order to match the high-multiplicity pp data.

In the context of this study, it is worth noting that some other hydro-based calculations have reported good agreement with a few observables of high-multiplicity events of small collision systems. A fluctuating proton impact-parameter-dependent glasma (IP-glasma) initial-state model coupled to viscous hydrodynamic simulations, followed by the hadronic cascade model UrQMD, could well reproduce the harmonic flow coefficients of pPb data at $\sqrt{s_{NN}} = 5.02$ TeV [37]. Another study [38] quantitatively matched the collective features of high-multiplicity event data of pPb collisions at the LHC and $(\mathrm{p}, \mathrm{d}, {}^3\mathrm{H})$Au collisions at the RHIC using a viscous hydrodynamic model. A common hydrodynamic origin for the experimentally observed flow of produced particles was suggested [39] for all (large or small) central collision systems (including pp, pPb, and PbPb) at the LHC by considering a generalized initial-condition calculation in the Glauber model at the subnucleonic level, followed by a hybrid model that combined preequilibrium dynamics with viscous fluid dynamical evolution and late-stage hadronic rescatterings.

On the other hand, some of the nonhydrodynamic models of particle production also qualitatively match certain bulk collective features of high-multiplicity pp events. The color glass condensate (CGC) effective theory also explains several experimental observations (including the azimuthal correlations) of high-multiplicity small collision systems. The particle-mass dependence of $\langle p_T \rangle$ and the p_T dependence of v_2 for pp collisions could be qualitatively reproduced using the IP-glasma model (based on the color glass condensate), followed by PYTHIA's Lund string fragmentation algorithm, with further tuning of the p_T-smearing fragmentation parameter in the default PYTHIA [40]. The literature also provides other sources of long-range rapidity correlations beyond hydrodynamic or CGC models in terms of initial-state physics processes. Several sources of such long-range azimuthal correlations have been discussed in Refs. [41,42]. The ALICE measurement of the $\langle p_T \rangle$ of charged particles as a function of N_{ch} (including particles with p_T up to 10 GeV/c) from pp collisions at 7 TeV could be well reproduced [31] by invoking the color reconnection mechanism in PYTHIA (while the EPOS3 model remains far away from the data). The MPI model, however, cannot explain [35] the dependence of $\langle p_T \rangle$ on $\langle N_{\mathrm{ch}} \rangle$ or provide alternate explanations of other important features of particle production in high-multiplicity pp collisions at 7 TeV when the p_T range is restricted to the range of interest for studying hydrodynamic collectivity.

The present study is consistent with the ALICE study [43] that observes the EPOS3 event generator is tuned to the LHC Run 1 data, to describe the inclusive transverse momentum spectrum for 13 TeV pp collisions reasonably well but not in detail. Similarly, no particle production model (hydrodynamic or nonhydrodynamic) could quantitatively match all of the collective features of the high-multiplicity pp data, while the high-multiplicity proton-nucleus data have been better matched by several models [37–40,44], including EPOS3. Thus, we conclude that the observed anomaly in particle production in high-multiplicity pp events at the LHC still remains unresolved, inviting further tuning of the existing models to obtain a quantitative description of the data.

ACKNOWLEDGMENTS

We thank Klaus Werner for providing us with the EPOS3 code. We also thank the members of the computing teams of KANNAD of the C&I Group of VECC for providing uninterrupted access to their facility for event generation.

[1] S. Z. Belenky and L. D. Landau, Nuovo Cimento Suppl. **3**, 15 (1956).
[2] I. Arsene *et al.* (BRAHMS Collaboration), Nucl. Phys. **A757**, 1 (2005).
[3] B. B. Back *et al.* (PHOBOS Collaboration), Nucl. Phys. **A757**, 28 (2005).
[4] J. Adams *et al.* (STAR Collaboration), Nucl. Phys. **A757**, 102 (2005).
[5] K. Adcox *et al.* (PHENIX Collaboration), Nucl. Phys. **A757**, 184 (2005).
[6] J. C. Collins and M. J. Perry, Phys. Rev. Lett. **34**, 1353 (1975).
[7] E. Shuryak, Phys. Rep. **61**, 71 (1980).
[8] V. Khachatryan *et al.* (CMS Collaboration), J. High Energy Phys. 09 (2010) 091.
[9] G. Aad *et al.* (ATLAS Collaboration), Phys. Rev. Lett. **116**, 172301 (2016).
[10] V. Khachatryan *et al.* (CMS Collaboration), Phys. Rev. Lett. **116**, 172302 (2016).
[11] V. Khachatryan *et al.* (CMS Collaboration), Phys. Lett. B **765**, 193 (2017).
[12] B. Ablev *et al.* (ALICE Collaboration), Phys. Lett. B **719**, 29 (2013).
[13] S. Chatrchyan *et al.* (CMS Collaboration), Phys. Lett. B **718**, 795 (2013).

[14] G. Aad *et al.* (ATLAS Collaboration), Phys. Rev. Lett. **110**, 182302 (2013).
[15] B. Ablev *et al.* (ALICE Collaboration), Phys. Lett. B **728**, 25 (2014).
[16] A. Adare *et al.* (PHENIX Collaboration), Phys. Rev. Lett. **114**, 192301 (2015).
[17] A. Adare *et al.* (PHENIX Collaboration), Nat. Phys., DOI: 10.1038/s41567-018-0360-0 (2018).
[18] K. Werner, I. Karpenko, and T. Pierog, Phys. Rev. Lett. **106**, 122004 (2011).
[19] P. Ghosh, S. Muhuri, J. Nayak, and R. Varma, J. Phys. G **41**, 035106 (2014).
[20] V. Khachatryan *et al.* (CMS Collaboration), Eur. Phys. J. C **72**, 2164 (2012).
[21] E. Schnedermann, J. Sollfrank, and U. W. Heinz, Phys. Rev. C **48**, 2462 (1993).
[22] P. Bozek, Eur. Phys. J. C **71**, 1530 (2011).
[23] R. Campanini and G. Ferri, Phys. Lett. B **703**, 237 (2011).
[24] A. Kisiel, Phys. Rev. C **84**, 044913 (2011).
[25] E. Shuryak and I. Zahed, Phys. Rev. C **88**, 044915 (2013).
[26] I. Bautista, A. F. Tellez, and P. Ghosh, Phys. Rev. D **92**, 071504(R) (2015).
[27] K. Werner, B. Guiot, I. Karpenko, and T. Pierog, Phys. Rev. C **89**, 064903 (2014).
[28] B. Ablev *et al.* (ALICE Collaboration), Eur. Phys. J. C **73**, 2662 (2013).
[29] G. Aad *et al.* (ATLAS Collaboration), Phys. Lett. B **758**, 67 (2016).
[30] A. M. Sirunyan *et al.* (CMS Collaboration), Phys. Rev. D **96**, 112003 (2017).
[31] B. Abelev *et al.* (ALICE Collaboration), Phys. Lett. B **727**, 371 (2013).
[32] I. G. Bearden *et al.* (NA44 Collaboration), Phys. Rev. Lett. **78**, 2080 (1997).
[33] N. Xu, Prog. Part. Nucl. Phys. **53**, 165 (2004).
[34] S. Chatrchyan *et al.*(CMS Collaboration), Eur. Phys. J. C **74**, 2847 (2014).
[35] S. Kar, S. Choudhury, S. Muhuri, and P. Ghosh, Phys. Rev. D **95**, 014016 (2017).
[36] T. Sjostrand, S. Mrenna, and P. Skands, J. High Energy Phys. 05 (2006) 026.
[37] H. Mntysaari, B. Schenke, C. Shen, and P. Tribedy, Phys. Lett. B **772**, 681 (2017).
[38] C. Shen, J.-F. Paquet, G. S. Denicol, S. Jeon, and C. Gale, Phys. Rev. C **95**, 014906 (2017).
[39] R. D. Weller and P. Romatschke, Phys. Lett. B **774**, 351 (2017).
[40] B. Schenke, S. Schlichting, P. Tribedy, and R. Venugopalan, Phys. Rev. Lett. **117**, 162301 (2016).
[41] K. Dusling, W. Li, and B. Schenke, Int. J. Mod. Phys. E **25**, 1630002 (2016).
[42] S. Schlichting and P. Tribedy, Adv. High Energy Phys. **2016**, 8460349 (2016).
[43] J. Adam *et al.* (ALICE Collaboration), Phys. Lett. B **753**, 319 (2016).
[44] S. Kar, S. Choudhury, S. Sadhu, and P. Ghosh, J. Phys. G **45**, 125103 (2018).